



Modeling of tritium transport in ceramic breeder single crystal

A. René Raffray, Seungyon Cho, Mohamed A. Abdou

Mechanical, Aerospace and Nuclear Engineering Department, University of California, Los Angeles, CA 90024-1597, USA

(Received 2 August 1993; accepted 7 January 1994)

Abstract

Simple existing models were found not to adequately reproduce recent tritium release data for LiAlO_2 single crystal, indicating the need for a more comprehensive model. To help understand and interpret the data, a new model, MISTRAL-SC, was developed, incorporating bulk diffusion as well as the four major surface processes, and allowing for the variation of surface activation energies with coverage and for the presence of H_2 in the purge. The model is described in this paper and an analysis of the single crystal data presented. Based on the analysis a bulk diffusion coefficient for tritium diffusing in LiAlO_2 is estimated and compared to previous estimated values from past experiments. Discrepancies are discussed and recommendations are proposed for values of the diffusion coefficient to be used in LiAlO_2 experiment and blanket analyses, and for future work.

1. Introduction

One of the key issues for ceramic breeder blankets is tritium release. The tritium generated in the ceramic breeder by neutron reactions with ^6Li and/or ^7Li is believed to be transported out of the breeder through a number of mechanisms [1]. As shown in Fig. 1, the bred tritium diffuses through the bulk in atomic form; it then diffuses along grain boundaries to the solid/gas interface where a number of surface processes occur, including desorption to and adsorption from the pores. The desorbed tritium then percolates along the open interconnected porosity to be finally convected away by the purge gas. The overall process can be slowed down (and the tritium inventory increased) by mechanisms such as chemical or radiation-induced trapping in the bulk.

A number of models have been developed which include some or all of the above mechanisms (e.g. by Federici et al. [1], and by Billone et al. [2]). However, in order to apply these models to the analysis of integrated experiments and/or of blanket situations, characterization of fundamental property data, such as the bulk diffusion coefficient and activation energies of surface processes, is required. Properties associated with individual release mechanisms can be best charac-

terized through experiments where the number of tritium transport mechanisms is minimized. For example, temperature-programmed desorption is a laboratory technique which enables the estimation of desorption activation energy and pre-exponential as described by Lord and Kittelberger [3].

Another technique involves tritium release measurements from ceramic breeder single crystal, which provides a method to eliminate the effect of pore diffusion and to minimize the effect of finite tritium concentration in the purge. In addition, by choosing large single crystals (for slow bulk diffusion) and measuring the tritium release in a purge with protium addition (for fast surface desorption), bulk diffusion would tend to be rate-controlling. The bulk diffusion pre-exponential and activation energy could then be estimated from the tritium release results by applying the solution to the simple diffusion equation with zero tritium concentration as the boundary condition at the single crystal surface.

For Li_2O , several such experiments have been done and values of the bulk diffusion coefficient estimated from the results tend to be quite consistent as summarized in Ref. [2]. However, for the ternary ceramics, single crystal experiments have been scarce. Most of the tritium release experiments have been done with

porous sintered pellets (polycrystals), involving all the tritium transport mechanisms. Values of the estimated diffusion coefficient for LiAlO_2 from such experiments, for example, range over several orders of magnitude indicating that the calculated “effective” diffusion coefficient in each case includes the effect of more than diffusion only.

Recently, sets of experimental data for tritium release from LiAlO_2 single crystal under constant temperature anneal and constant heating rate conditions were published by Botter et al. [4], and by Kopasz et al. [5]. Application of the simple models available for pure diffusion, pure desorption and diffusion/desorption to the analysis of these results indicated the need for a more comprehensive model in order to be able to interpret the results. Given the scarcity of such single crystal data, interpreting and understanding these existing results in order to derive estimates of fundamental property data, such as the bulk diffusion coefficient, would be very beneficial for subsequent analysis of LiAlO_2 blanket or test modules.

To help in this endeavor, a new, more comprehensive model for tritium release from ceramic breeder single crystal was developed and applied to the experimental data. The model would also provide a tool for the analysis of future experiments on tritium release from lithium ceramic single crystal. In addition, the analysis would help to determine key property data that need to be characterized and to focus future experimental activities accordingly.

This paper describes the results of this activity. First, the experimental results for LiAlO_2 single crystal are briefly described. Application of the simple existing models to the analysis of the data is then discussed. Next, the new model proposed here is described; the results of the data analysis using the new model and existing property data are then presented. An assessment and discussion of bulk diffusion and surface

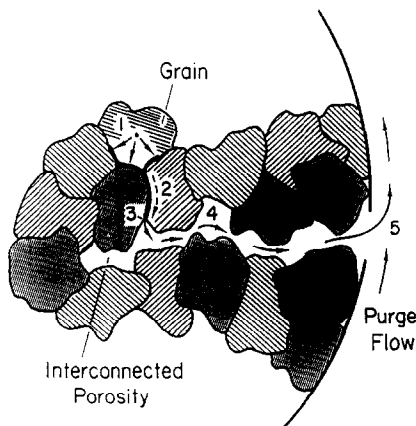
property data including those estimated from the data fit follows. Finally, conclusions are drawn and recommendations proposed.

2. Experimental results

Over the last couple of years, experimental results for tritium release from LiAlO_2 single crystals have been presented in the literature [4,5]. These experiments have been performed at CEA/CEN Saclay as part of a larger matrix of types of LiAlO_2 , including pure and doped single crystal and sintered pellet samples. The LiAlO_2 samples were first irradiated at low temperature for ~ 10 h in the OSIRIS reactor under a thermal neutron flux of about 10^{18} n/m² s. Out-of-reactor tritium release experiments were then carried under constant temperature and constant heating rate conditions. Typical tritium release results obtained under these conditions for the 2 mm pure LiAlO_2 single crystals are shown in Figs. 2 and 3.

Fig. 2 shows an example of the tritium release under successive constant temperature anneals of 538, 777 and 950°C. The irradiated sample was introduced in a furnace preheated to 538°C and the tritium release to a carrier gas of Ar + 0.1% H₂ was measured by a proportional counter. The temperature was raised to each of the two higher values (777 and 950°C) after the tritium release had decreased to about the baseline value. A small release peak is observed at 538°C followed by a large peak at 777°C and another small one at 950°C.

Fig. 3 shows an example of the tritium release results under constant heating rate conditions of 0.5 K/min. In this case, the irradiated sample was placed in the furnace with Ar + 0.1% H₂ as purge gas and the temperature was raised linearly with time from about 10 to 950°C. The tritium release was measured down-



Mechanisms of Tritium Transport

- 1) Intragranular Diffusion
- 2) Grain Boundary Diffusion
- 3) Surface Adsorption/Desorption
- 4) Pore Diffusion
- 5) Purge Flow Convection

Fig. 1. Schematic of tritium transport mechanisms in lithium ceramics.

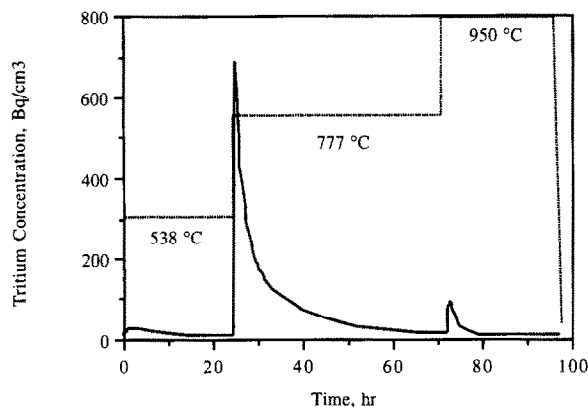


Fig. 2. Example of tritium release from 2 mm LiAlO₂ single crystal under constant temperature anneals [5].

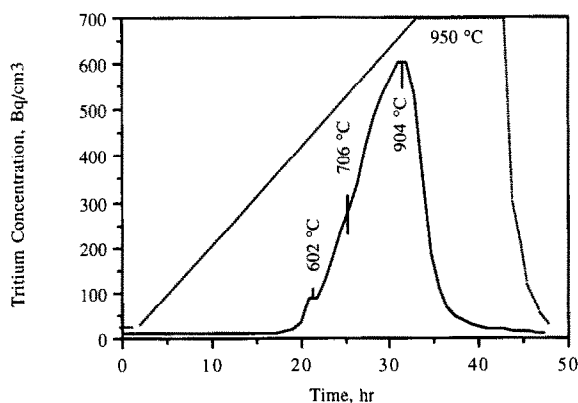


Fig. 3. Example of tritium release from 2 mm LiAlO₂ single crystal under a 0.5 K/min constant heating rate condition [5].

stream by a proportional counter. The tritium release reaches a maximum value at about 904°C and then starts decreasing. During the ramp-up, two small shoulders in the curve seem to indicate the presence of several bulk or surface activated sites with different activation energies.

3. Available models

If the tritium transport mechanisms are assumed to be controlled by diffusion or desorption (first- or second-order) or a combination of diffusion and desorption, there are simple existing models which can be used for the analysis. Table 1 summarizes these models in terms of the governing equations, the boundary conditions and the final analytical expression for the fractional release rate. From the table, C is the tritium concentration in the bulk, D the bulk diffusion coefficient, K_d the first-order desorption coefficient, K_r the second-order desorption coefficient, a the single-crystal

radius, A the area to volume ratio and F the tritium release fraction. Note that for the desorption cases, it is assumed that the surface coverage is proportional to the bulk concentration.

These simple models were used to try to reproduce the experimental tritium release results. A more detailed account of the comparison can be found in Ref. [6]. Here, the findings are summarized and example results shown as illustration.

3.1. Diffusion control

Typically, the diffusion control expression is used to analyze tritium release from lithium ceramic single crystals. The combination of large single crystals (for slow diffusion) and release to a purge with protium addition (for fast surface desorption) tends to result in diffusion as the rate-controlling mechanism. The results for Li₂O summarized in Ref. [2] were obtained by applying the diffusion-control expression to experimental results.

The expression was applied to the LiAlO₂ single-crystal tritium release results under constant temperature anneals, shown in Fig. 2. Comparisons of the calculated fractional tritium release for different bulk diffusion coefficients to the experimental results were done for each temperature anneal. The initial tritium inventory, C_0 , of Table 1 was estimated for each case by integrating the subsequent tritium release history assuming negligible tritium inventory at the end of the highest-temperature anneal (950°C).

For example, Fig. 4 shows a comparison of the calculations with experimental results for the 538°C anneal case. The tritium release cannot be properly reproduced with any value of the bulk diffusion coefficient, D . If D is chosen to reproduce the release fraction at the end of the anneal, the initial release fraction slope is much steeper than the experimental one. D could be lowered to reproduce this initial slope, but the release fraction at the end of the anneal is then much lower than the experimental one. Similarly, the experimental results for the 950°C anneal case could not be properly reproduced with any value of D . However, for the 777°C anneal case, a diffusion coefficient of 2×10^{-12} m²/s was found to reasonably reproduce the results.

Overall, however, it is clear that the diffusion control expression falls short in modeling the constant temperature tritium release results. Some other tritium mechanism(s) must be considered.

3.2. Desorption control

The fractional release expressions for first-order and second-order desorption control from Table 1 were also applied to the constant temperature tritium re-

Table 1
Analytical models for calculating tritium release from a spherical single crystal

Diffusion control	Desorption control (first order)	Desorption control (second order)	Diffusion/desorption control
$\frac{\partial C}{\partial t} = D \frac{1}{r^2} \frac{\partial}{\partial r} \left(r^2 \frac{\partial C}{\partial r} \right)$	$\frac{\partial C}{\partial t} = -K_d AC$	$\frac{\partial C}{\partial t} = -K_r AC^2$	$\frac{\partial C}{\partial t} = D \frac{1}{r^2} \frac{\partial}{\partial r} \left(r^2 \frac{\partial C}{\partial r} \right)$
$\frac{\partial C}{\partial r} = 0$ at $r = 0$	$C = C_0$ at $t = 0$	$C = C_0$ at $t = 0$	$\frac{\partial C}{\partial r} = 0$ at $r = 0$
$C = 0$ at $r = a$	$J = K_d C$ at $r = a$	$J = K_r C^2$ at $r = a$	$-D \frac{\partial C}{\partial r} = K_d C$ at $r = a$
$C = C_0$ at $t = 0$			$C = C_0$ at $t = 0$
$F = 1 - \frac{6}{\pi^2} \sum_{n=1}^{\infty} \frac{1}{n^2} e^{-n^2 \pi^2 D t / a^2}$	$F = 1 - e^{-K_d A t}$	$F = \frac{C_0 K_r A t}{C_0 K_r A t + 1}$	$F = 1 - \frac{\sum_{n=1}^{\infty} \frac{1/\alpha_n}{(\alpha_n^2 + h^2) a + h} e^{-D \alpha_n^2 t}}{\sum_{n=1}^{\infty} \frac{1/\alpha_n}{(\alpha_n^2 + h^2) a + h}}$

A: area to volume ratio ($= 3/a$), $h = K_d/D - 1/a$, α_n ($n = 1, 2, \dots$): root of $[\alpha \cos(\alpha a) + h \sin(\alpha a) = 0]$.

lease results. As an example, Fig. 5 shows the comparison of the experimental results with the modeling results for the fractional tritium release based on first-order desorption for the 538°C temperature anneal case. The modeling results are shown for different values of the desorption coefficient. A reasonable reproduction of the experimental results is not possible for the 538°C case for any values of the desorption coefficient. Similarly, for the 950°C case, the results could not be reasonably reproduced while for the 777°C case, the reproduction of the experimental results for a chosen desorption coefficient, although not ideal, was certainly better than for the other cases.

For second-order desorption, reproduction of the experimental results for the 538°C anneal case is also impossible for any value of the desorption coefficient,

as shown in Fig. 6. However, the initial slope of the fractional release could be reasonably reproduced for the 777 and 950°C cases. The second-order desorption coefficient can be chosen to reproduce the results very well up to a time of about 0.5×10^5 s within the temperature anneal, the calculated fractional tritium release slope then diverging to the lower side of the experimental results.

The experimental results also include tritium release under constant heating rate conditions, as shown in Fig. 3. Typically, such experiments are done on samples which have been saturated with a single gaseous adsorbate and the analysis of the results can help determine desorption activation energies and pre-exponentials (temperature-programmed desorp-

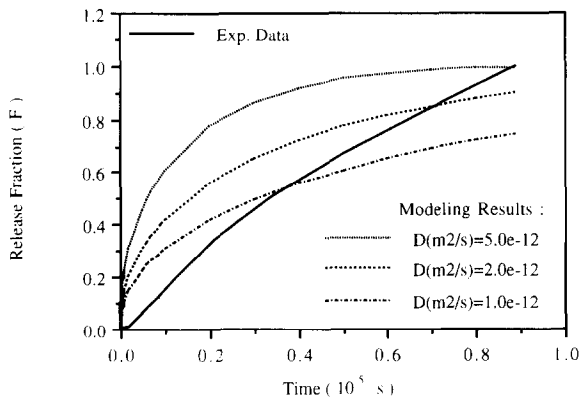


Fig. 4. Comparison of experimental fractional tritium release at 538°C with modeling results based on the diffusion control expression for different diffusion coefficients.

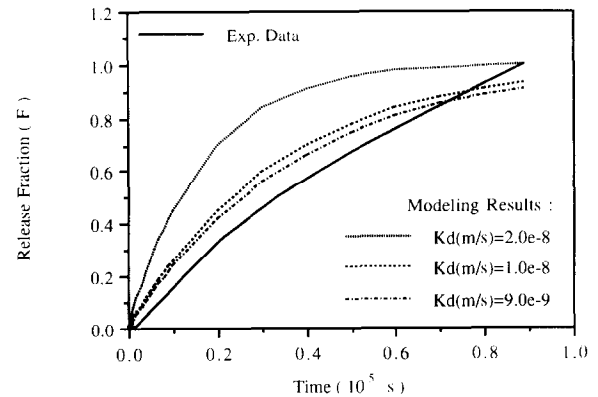


Fig. 5. Comparison of experimental fractional tritium release at 538°C with modeling results based on first-order desorption control expression for different desorption coefficients.

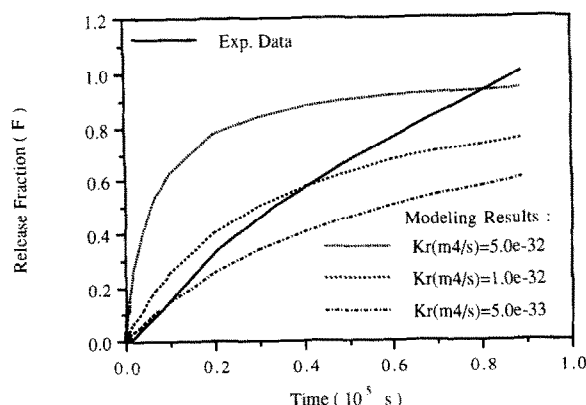


Fig. 6. Comparison of experimental fractional tritium release at 538°C with modeling results based on second-order desorption control expression for different desorption coefficients.

tion, TPD [3]). For example, the desorption equation expressed in terms of the surface coverage, θ , is:

$$\frac{d\theta}{dt} = -A_{\text{des}}\theta^{n_d} \exp(-n_d E_{\text{des}}/RT), \quad (1)$$

where A_{des} is the pre-exponential, E_{des} is the desorption activation energy associated with each desorbing atom or radical, n_d is the order of desorption, R is the gas constant and T is the temperature.

For a constant heating rate experiment, $dT = \beta dt$ where β is the linear heating rate. Usually, such an experiment is run with fast pumping so that there is negligible resorption and the gaseous desorbate partial pressure, P , is measured as a function of the temperature. P is then proportional to $-(d\theta/dt)$. Setting $dP/dT = 0$ at the maximum of the release and differentiating yields [3]:

$$\ln\left(\frac{T_m^2 \theta_m^{n_d-1}}{\beta}\right) = \frac{n_d E_{\text{des}}}{RT_m} + \ln\left(\frac{E_{\text{des}}}{A_{\text{des}} R}\right), \quad (2)$$

where T_m and θ_m are the temperature and coverage at the maximum release rate. The interesting point about this equation is that T_m is independent of θ_m for first-order desorption ($n_d = 1$) but depends on θ_m for higher order desorption ($n_d > 1$).

Ref. [5] describes an attempt to use Eq. (2) to estimate activation energies for the tritium desorption from the LiAlO_2 single crystal. First order desorption was assumed based on the presence of protium in the purge which would swamp the surface. The tritium release results for constant heating rates of 0.5 and 2 K/min were assumed to consist of desorption from three types of sites resulting in two small shoulders in addition to the maximum peak. For example, Fig. 4 shows shoulders at about 602 and 706°C and a maximum at 904°C for the tritium release curve under 0.5

K/min. Activation energies estimated from these shoulders using Eq. (2) fall within the general range estimated from Fischer and Johnson's heat of adsorption results for water desorption from LiAlO_2 [7].

Some concern exists, however, in that use of Eq. (2) for this case stretches the limits of its applicability. Eq. (2) was derived by assuming that $d\theta/dt$ is only dependent on the desorption flux which infers that all the desorbate concentration is on the surface. If tritium is produced inside the sample, as in the case of the LiAlO_2 single crystal, the bulk concentration is likely to be at least of the same order if not significantly greater than the surface concentration. Eq. (1) should then include an extra term on the right-hand side to account for the tritium flux coming from the bulk to the surface. The magnitude of this flux relative to the desorption flux would determine the time-dependent behavior of θ .

To get around this problem, one could assume that, if diffusion is fast, the bulk concentration can be normalized through a simple geometrical factor to estimate the surface coverage and the whole tritium concentration in the single-crystal can then be considered instead of $d\theta/dt$ in Eq. (2). Even if this assumption holds, the presence of protium addition to the purge would complicate matters as the surface coverage would be dependent on it and it is not clear whether the tritium concentration in the bulk could then be used to estimate the surface coverage.

The presence of protium in the purge, although enhancing tritium desorption through surface swamping, is also an extra element not considered in the derivation of Eq. (2). Tritium desorption would directly depend on the protium coverage which itself varies with temperature. Thus, it is not clear that assumption of a constant value of protium coverage leading to a quasi-first order desorption is reasonable. Finally, the desorption activation energy is a function of coverage [7], which was also not included in the derivation of Eq. (2).

Derivation of an expression similar to Eq. (2) but including all the elements present in the single-crystal experiment can be quite complex even when using simplifying assumptions. This can be illustrated by expressing Eq. (1) for the single-crystal case, based on second-order adsorption/desorption.

$$\left(\frac{dC}{dt} \frac{1}{A} + \frac{d\theta_T}{dt}\right) = -A_{\text{des}}\theta_T(2\theta) \exp(-2E_{\text{des}}/RT), \quad (3)$$

where C is the tritium bulk concentration, A is a geometry parameter, and θ_T and θ are the tritium and total coverages respectively. For simplicity, the protium

coverage is assumed much higher than the tritium coverage and $\sim \theta$, which can be calculated from:

$$\frac{d\theta}{dt} = -A_{\text{des}}\theta^2 \exp(-2E_{\text{des}}/RT) + A_{\text{ads}}P_{\text{H}}(1-\theta)^2 \exp(-2E_{\text{ads}}/RT), \quad (4)$$

where A_{ads} is the pre-exponential for adsorption, P_{H} is the protium partial pressure in the purge and E_{ads} is the adsorption activation energy associated with each adsorbing atom or radical. E_{ads} can be reasonably assumed to be approximately constant over a range of coverage. However, E_{des} depends on coverage. Ref. [7] lists five values of the heat of adsorption, Q_{ads} , for the $\text{LiAlO}_2/\text{H}_2\text{O}$ system for five different coverages (0.001 to 0.1). These heat of adsorption values are determined by the most active sites at the given coverage. For calculation purposes, let us assume that Q_{ads} is a continuous function of θ . For a constant E_{ads} , E_{des} ($= Q_{\text{ads}} + E_{\text{ads}}$) would follow the same variation with coverage which can be expressed as:

$$E_{\text{des}} = C_1 - C_2 \ln \theta, \quad (5)$$

where C_1 and C_2 are constants.

At the peak of the tritium release versus temperature curve, the right-hand side of Eq. (3) can be differentiated with respect to temperature and set to zero. The whole process is quite complicated, however, as E_{des} should be substituted from Eq. (5) and the variation of θ with temperature is determined from Eq. (4) with $dT = \beta dt$. A simple analytical solution is no longer possible. So many variables enter the equations that the usefulness of even a numerical solution is marginal in helping to determine A_{des} and E_{des} , unless E_{ads} and A_{ads} are known and E_{des} is a known function of θ , such as expressed in Eq. (5), for example, for which constants C_1 and C_2 can be calculated.

In summary, one has to be very careful when applying the simple conventional TPD equations to situations where their validity is not known to be satisfied.

3.3. Diffusion / desorption control

The analytical expression for the fractional release of tritium based on a combination of diffusion and first order desorption (see Table 1) was also used to try to reproduce the constant temperature tritium release results by varying the diffusion and/or desorption coefficients. The fits are generally better than for the diffusion control or desorption control cases. It is still not possible, however, to adequately reproduce the 538°C anneal case, as shown in Fig. 7. The data fit for the 777 and 950°C cases were found to be better particularly for the former one.

Overall, however, when the particular experimental conditions including tritium generation in the bulk and

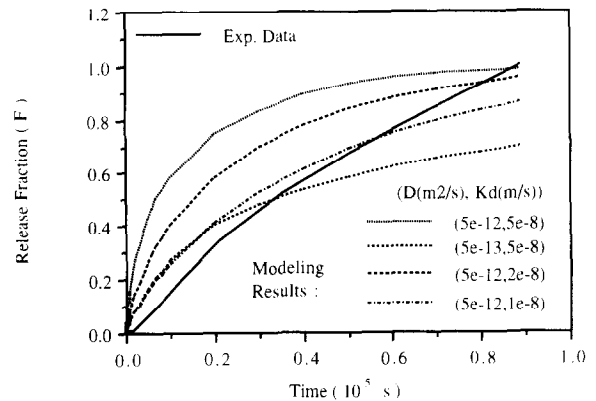


Fig. 7. Comparison of experimental fractional tritium release at 538°C with modeling results based on the diffusion/first-order desorption control expression for different diffusion and desorption coefficients.xxxxx

protium addition to the purge, and the fact that the activation energy for desorption varies with the coverage are taken into consideration, the usefulness of the simple analytical expressions shown in Table 1 is limited. Certainly, by assuming that several independent variables can be varied, such as more than one pre-exponential and activation energy of desorption per temperature anneal, an acceptable reproduction of the experimental data can be obtained [5]. However, application of the results for analysis of tritium release from LiAlO_2 over a range of blanket conditions is limited.

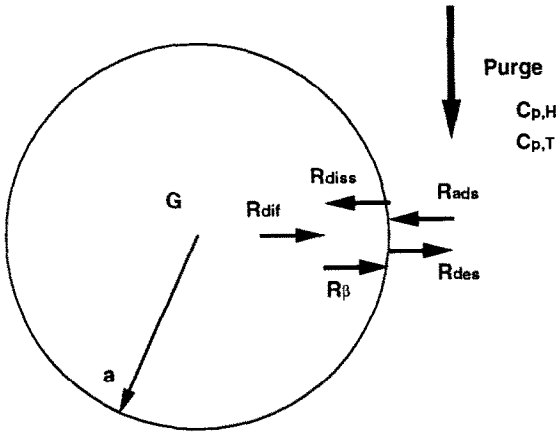
At this stage, a new, more comprehensive model would be very useful to better understand the tritium transport behavior in single crystals by more thoroughly accounting for the transport mechanisms and operating conditions. The model would help in estimating property data such as diffusion coefficients and activation energies of surface processes which can be used for blanket analysis. Such a model is proposed and described in the next section.

4. Proposed model: MISTRAL-SC

Analysis of the single-crystal tritium release results with the simple analytical models indicates that tritium release from the ceramic single crystal is not controlled by only one simple mechanism but by a combination of several mechanisms including surface reactions. To better understand the tritium transport mechanisms involved, a comprehensive model which includes surface processes as well as bulk diffusion is proposed.

A schematic of the model is shown in Fig. 8. It includes the following transport processes:

(1) production of tritium in the single crystal,



- a = Single crystal radius**
- G = Tritium generation rate in bulk**
- R_{dif} = Tritium bulk diffusion flux**
- Surface fluxes:**
 - R_{diss} = Dissolution flux**
 - R_β = Bulk to surface flux**
 - R_{des} = Desorption flux**
 - R_{ads} = Adsorption flux**
- C_{p,H} = Concentration of protium atoms in purge**
- C_{p,T} = Concentration of tritium atoms in purge**

Fig. 8. Schematic of proposed model for tritium transport in ceramic breeder single crystal.

- (2) diffusion of tritium to the surface in the form of T⁺ through the bulk,
- (3) surface processes at the solid/gas interface, and
- (4) removal of the tritium compounds out of the breeder by purge gas stream.

The single crystal is assumed spherical and the total coverage surface area is assumed to be that of a sphere. This is one important simplification when modeling a single-crystal geometry instead of a porous sintered pellet geometry where the specific surface area must be determined experimentally. The model allows for the presence of protium in the purge and considers both tritium and protium as desorbate and adsorbate under the assumption of second order adsorption/desorption. Chemical and/or radiation trapping of tritium inside the bulk are not considered in the absence of reliable data. This is probably reasonable for the LiAlO₂ case, but might not be for the Li₂O case where LiOT formation is more likely to occur and cause bulk trapping of the tritium under certain conditions.

The model is based on the MISTRAL methodology, developed by Federici et al. [1], which was specifically

applied to the single crystal situation and is called MISTRAL-SC (SC = single crystal). The equations used in MISTRAL-SC are summarized below, the symbols being described in the Nomenclature section.

4.1. Bulk-diffusion equation

The diffusion equation for tritium in a single crystal with spherical geometry can be written as follows:

$$\frac{\partial C(r, t)}{\partial t} = D(T) \frac{1}{r^2} \frac{\partial}{\partial r} \left(r^2 \frac{\partial C(r, t)}{\partial r} \right) + G. \quad (6)$$

The diffusion coefficient in the single crystal is given by

$$D(T) = D_0 \exp(-E_{\text{diff}}/RT). \quad (7)$$

The boundary conditions are

$$\frac{\partial C}{\partial r} = 0 \quad \text{at } r = 0, \quad (8)$$

$$-D \frac{\partial C}{\partial r} = R_{\beta(T)} - R_{\text{diss}(T)} \quad \text{at } r = a, \quad (9)$$

where R_{β(T)} and R_{diss(T)} are the tritium flux from the bulk to surface and dissolution flux respectively, as illustrated in Fig. 8.

4.2. Rate equations at the surface

The four surface fluxes are assumed to be activated and functions of the surface coverage. In the absence of experimental data, it seems reasonable to assume that the activation energy for each of these surface processes is the same for both tritium (T) and protium (H) species. The following rate equations govern the T and H coverage.

$$N_s \frac{d\theta_j}{dt} = R_{\beta(j)} - R_{\text{diss}(j)} + \sum_i \gamma_i^j R_{\text{ads}}^i - \sum_i \gamma_i^j R_{\text{des}}^i, \quad (10)$$

where j represents the adsorbed species, T or H, and γ_i^j is the number of atoms of species j which adsorbs or desorbs per each gas molecules of species i. In the model, all four surface fluxes are considered for T whereas only the adsorption and desorption fluxes are considered for H to account for the effect of H swamping on the coverage. The four fluxes can be described as follows:

(1) Adsorption flux from the purge to the surface (assuming dissociative adsorption):

$$R_{\text{ads}}^i(\theta, t) = k_{\text{ads}}^i(T, \theta) C_{p,i}(t) (1 - \theta)^2, \quad (11)$$

where C_{p,i} is the concentration in the purge of H or T bearing molecules and the factor (1 - θ)², where θ = θ_T + θ_H, accounts for the fact that two empty surface sites are required for each part of the dissociated molecule to chemisorb. Based on Trapnell and Hay-

ward [7] and Ref. [1], the rate constant $k_{\text{ads}}^i(T, \theta)$ for dissociative adsorption can be estimated from:

$$k_{\text{ads}}^i(T, \theta) = \frac{\sigma N_z}{\sqrt{8 \times 10^{-3} \pi}} \sqrt{\frac{RT}{M^i}} \exp(-2E_{\text{ads}}/RT), \quad (12)$$

where E_{ads} is the activation energy associated with each hydrogen atom or radical adsorbing on the surface and the factor 2 in the exponent accounts for second-order dissociative adsorption whereby two hydrogen atoms and/or radicals adsorb from each adsorbate molecule. The pre-exponential is the product of the rate at which molecules from the gas phase would strike a site area and the condensation coefficient, σ , which represents the fraction of molecules hitting the surface that stick to the surface.

(2) Desorption flux from the surface to the purge:

$$R_{\text{des}}^i(\theta, t) = k_{\text{des}}(T, \theta)\theta_q\theta_j, \quad (13)$$

where the rate constant $k_{\text{des}}(T, \theta)$ for associated desorption can be estimated from [8,9,1]:

$$k_{\text{des}}(T, \theta) = \frac{N_s N_z RT}{2N_{\text{av}} h} \exp(-2E_{\text{des}}/RT). \quad (14)$$

For energetic reasons, the desorption flux is always in the form of molecules [10]. A pair of adsorbed atoms and/or radicals (with corresponding coverages θ_q and θ_j) combines and desorbs as molecular species i , where q and j can be T or H. E_{des} is the desorption activation energy associated with each atom or radical on the surface and the factor 2 in the exponent accounts for second-order desorption.

(3) Flux of tritium atoms entering the surface from the bulk:

$$R_{\mathcal{A}(T)}(\theta, t) = k_{\mathcal{A}(T)}C(a, t)(1 - \theta), \quad (15)$$

where the factor $(1 - \theta)$ implies that there must be one empty site at the surface for the diffusing atom to reach the surface, and $k_{\mathcal{A}(T)}$ is given by:

$$k_{\mathcal{A}(T)} = \beta_0 \exp(-E_{\mathcal{A}}/RT), \quad (16)$$

and, from Pick and Sonnenberg [10], β_0 can be estimated from the vibration frequency at the surface ($\sim 10^{13} \text{ s}^{-1}$) as:

$$\beta_0 \sim 10^{13} / \sqrt{N_s}. \quad (17)$$

(4) Dissolution flux of adsorbed tritium atoms entering the bulk:

$$R_{\text{diss}(T)}(\theta, t) = k_{\text{diss}(T)}\theta_T, \quad (18)$$

where, by analogy to the desorption pre-exponential, the rate constant $k_{\text{diss}(T)}$ is expressed as [1]:

$$k_{\text{diss}(T)} = \frac{N_s N_z RT}{2N_{\text{av}} h} \exp(-E_{\text{diss}}/RT). \quad (19)$$

At each time step, the net tritium release rate, R_T (atoms/s), can be expressed in terms of the tritium desorption flux (Eq. (13)) minus the tritium adsorption flux (Eq. (11)), as follows:

$$R_T = \left[k_{\text{des}}2(\theta_H + \theta_T)\theta_T - (k_{\text{ads}}^{\text{HT}}C_{\text{p,HT}} + 2k_{\text{ads}}^{\text{T}_2}C_{\text{p,T}_2})(1 - \theta)^2 \right] A_s, \quad (20)$$

where A_s is the surface area of the single crystal. $C_{\text{p,HT}}$ and $C_{\text{p,T}_2}$ are the concentrations of either the reduced (HT, T_2) or oxidized (HTO, T_2O) forms of the species.

The concentration of protium atoms in the purge, $C_{\text{p,H}}$, can be estimated from its volume fraction in the purge, $V_{F,H}$, and the purge pressure, P , as follows:

$$C_{\text{p,H}} = 2V_{F,H} \frac{PN_{\text{av}}}{RT}, \quad (21)$$

where the factor 2 is used for converting from molecules to atoms.

There are also tritium species in the purge in particular on the downstream side of the single crystal due to the tritium desorbing on the upstream side of the single crystal. The average concentration of tritium atoms in the purge, $C_{\text{p,T}}$, can be estimated from the purge volume flow rate, V_p , and the tritium release rate, R_T , from Eq. (20):

$$C_{\text{p,T}} = 0.5 \frac{R_T}{V_p}, \quad (22)$$

where the factor 0.5 is used for averaging over the whole single crystal.

Since the available data are not sufficient to describe the kinetics of the chemical reactions in the purge, the reactions among the molecular species are assumed to be fast enough for chemical equilibrium to be maintained. For example, for the reduced species of T_2 , HT and H_2 , the following relationship holds based on the equilibrium constant, K_{eq} .

$$\frac{(C_{\text{p,HT}})^2}{C_{\text{p,T}_2}C_{\text{p,H}_2}} = K_{\text{eq}}, \quad (23)$$

Based on conservation of atoms, the concentrations of $C_{\text{p,T}_2}$ and $C_{\text{p,H}_2}$ are given by:

$$C_{\text{p,T}_2} = (C_{\text{p,T}} - C_{\text{p,HT}})/2, \quad (24)$$

$$C_{\text{p,H}_2} = (C_{\text{p,H}} - C_{\text{p,HT}})/2. \quad (25)$$

Substituting for $C_{\text{p,T}_2}$ and $C_{\text{p,H}_2}$ from Eqs. (24) and (25) in Eq. (23) gives:

$$(C_{\text{p,HT}})^2 = K_{\text{eq}} \frac{(C_{\text{p,T}} - C_{\text{p,HT}})}{2} \frac{(C_{\text{p,H}} - C_{\text{p,HT}})}{2}. \quad (26)$$

From Ref. [11], K_{eq} is ~ 4 . The expression for $C_{p,HT}$ can then be expressed as:

$$C_{p,HT} = \frac{C_{p,T}C_{p,H}}{C_{p,T} + C_{p,H}} \quad (27)$$

The concentrations of molecular species T_2 and H_2 in the purge can be obtained by substituting for $C_{p,HT}$ from Eq. (27) in Eqs. (24) and (25). C_{p,T_2} and C_{p,H_2} can then be expressed as:

$$C_{p,T_2} = \frac{1}{2} \frac{(C_{p,T})^2}{C_{p,T} + C_{p,H}}, \quad (28)$$

$$C_{p,H_2} = \frac{1}{2} \frac{(C_{p,H})^2}{C_{p,T} + C_{p,H}} \quad (29)$$

The concentration of hydrogen atoms, $C_{p,H}$, is estimated from the composition of the purge gas, as shown in Eq. (21). The concentration of tritium atom, $C_{p,T}$, can be derived from the total tritium released from the single crystal, as shown in Eq. (22). Substituting for R_T from Eq. (20) and for $C_{p,HT}$ and C_{p,T_2} from Eqs. (27) and (28) in Eq. (22) gives:

$$C_{p,T} = \frac{A_s}{2V_p} \left[2k_{des}\theta\theta_T - \left(k_{ads}^{HT}C_{p,H}C_{p,T} + k_{ads}^{T_2}(C_{p,T})^2 \right) \frac{(1-\theta)^2}{C_{p,T} + C_{p,H}} \right] \quad (30)$$

This is a quadratic equation which can be solved for $C_{p,T}$ in terms of $C_{p,H}$, θ and other parameters. The solution of this quadratic equation for $C_{p,T}$ is coupled with the rate equations (Eq. (10)) and solved numerically. The numerical scheme used is described briefly in the next section.

4.3. Numerical schemes for solving the governing equations

The governing equations consist of parabolic partial differential equations and stiff ordinary differential equations (rate equations). One of the most important steps towards the development of an efficient and accurate computer code is the device of the numerical techniques to solve the system of governing differential equations and associated initial and boundary conditions. The overall numerical scheme used for the solution is based on the well tested scheme for MISTRAL [1] and is briefly described here. A more detailed explanation of the numerical solution can be found in Ref. [6].

The diffusion equation for the single crystal is solved by using the Crank–Nicholson implicit finite difference scheme because of its unconditional stability even for a

large time step. An average of the central difference expressions for the first and second derivative terms at two time steps is applied for the spatial derivative. For the time derivative, a forward Euler approximation was used. The system of rate equations, which comes from coupling the surface region with the purge and bulk regions, is solved by the LSODE solver based on the GEAR's method. Rate equations describing the kinetics of thermally activated surface phenomena are typical examples of "stiff" problems involving rapidly decaying transient solutions. The algorithm of GEAR's method adjusts both the order (up to seven) and the mesh size to produce the desired local truncation error level, is self-starting and is particularly suited for dealing with "stiff" differential equations.

In order to use the numerical scheme more conveniently and more distinctively, the governing equations were first nondimensionalized in a similar way to that described in Ref. [1]. The model was then coded and verified based on reproducing simple analytical cases, such as those shown in Table 1. For example, the constant temperature tritium release history, $F(t)$, for a sphere with tritium generated at the rate, G , at time zero and for diffusion control is given by:

$$J(t) = \frac{Ga}{3} - \frac{2Ga}{\pi^2} \sum \frac{1}{n^2} \exp\left(\frac{-n^2\pi^2 t}{\tau}\right), \quad (31)$$

$$F(t) = \frac{J(t)}{J(\infty)} = 1 - \frac{6}{\pi^2} \sum \frac{1}{n^2} \exp\left(\frac{-n^2\pi^2 t}{\tau}\right), \quad (32)$$

where $J(t)$ is the flux from the surface to the purge stream at time t .

The same case was modeled using MISTRAL-SC. The tritium concentration in the purge was set to zero. The adsorption and desorption fluxes were excluded and the tritium flux out of the crystal was set by the

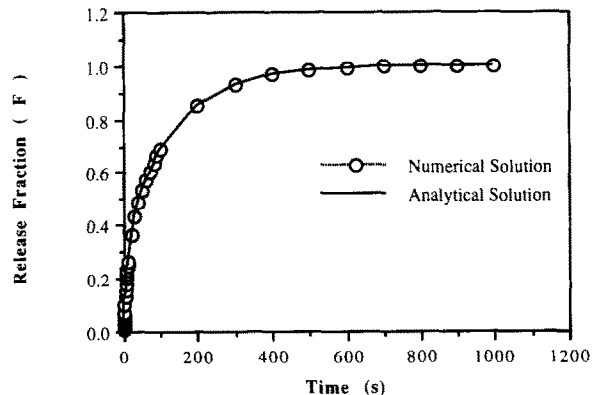


Fig. 9. Comparison of example code verification case for diffusion-control tritium release from a lithium ceramic sphere at constant temperature and for a constant tritium generation rate.

difference between R_β and R_{diss} . In order to artificially produce a diffusion-control situation, the bulk-to-surface flux activation energy was set very low while the dissolution flux activation energy was set high. The tritium generation and sphere radius used were similar to those from Ref. [4] and a typical diffusion coefficient was used. The results from MISTRAL-SC compared well with the analytical results from Eq. (32), as shown in Fig. 9. The code was then used to analyze the LiAlO_2 single crystal results.

5. Existing property data

In order to apply the code to the analysis of the single crystal experimental data, several parameters must be specified including the activation energies of the different surface processes and the bulk diffusion coefficient. Although all the specific activation energies for the surface processes illustrated in Fig. 8 have not been determined experimentally for LiAlO_2 , experimental data on the heat of adsorption, adsorption activation energy and energy of solution are available.

Fischer and Johnson [7] have determined experimentally the heat of adsorption as a function of coverage for the $\text{LiAlO}_2/\text{H}_2\text{O}$ system at a temperature of about 500°C . In the single crystal experiment, the system is closer to the $\text{LiAlO}_2/\text{H}_2$ case. However, evidence suggests that even for the latter system, desorption would occur as water [8]. Fischer [13] also indicated from his experiments that the desorption kinetic parameters for the $\text{LiAlO}_2/\text{H}_2\text{O}$ system are very similar to those for the $\text{LiAlO}_2/\text{H}_2$ system. Thus, in the absence of data for the specific $\text{LiAlO}_2/\text{H}_2$ system, it seems reasonable to use the heat of adsorption data from Ref. [7] for the LiAlO_2 analysis and to verify the

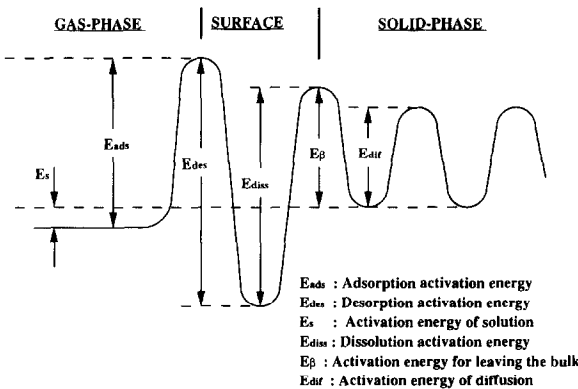


Fig. 10. Potential energy diagram for atomic and molecular hydrogen at the surface.

Table 2

Reference property data and parameters assumed in the analysis

Material	LiAlO_2 single crystal												
Sample radius	1 mm												
Purge flow													
Composition	Ar + 0.1% H_2												
Pressure	1 atm												
Flow rate	$5 \times 10^{-7} \text{ m}^3/\text{s}$												
Number of surface sites (N_s)	10^{19} sites/ m^2												
Condensation coefficient (σ)	4												
Number of adjacent sites (N_2)	4												
Bulk ads. pre-exp. factor (β_0)	$\frac{1 \times 10^{13}}{\sqrt{N_s}} \text{ m}$												
Surface activation energies													
Adsorption (E_{ads})	15 kJ/mol [14]												
Solution (E_{s})	23 kJ/mol [14]												
Desorption (E_{des})	$E_{\text{ads}} + Q_{\text{ads}}$												
Bulk adsorption (E_{β})	$E_{\text{dif}} + E_{\text{ads}}$												
Dissolution (E_{diss})	$E_{\text{s}} + E_{\beta} + Q_{\text{ads}}$												
Heat of adsorption (Q_{ads}) as a function of surface coverage, θ	<table border="1"> <thead> <tr> <th>θ</th> <th>$2Q_{\text{ads}}$ [7]</th> </tr> </thead> <tbody> <tr> <td>0.001</td> <td>360 kJ/mol</td> </tr> <tr> <td>0.0032</td> <td>290 kJ/mol</td> </tr> <tr> <td>0.01</td> <td>220 kJ/mol</td> </tr> <tr> <td>0.032</td> <td>150 kJ/mol</td> </tr> <tr> <td>0.1</td> <td>80 kJ/mol</td> </tr> </tbody> </table>	θ	$2Q_{\text{ads}}$ [7]	0.001	360 kJ/mol	0.0032	290 kJ/mol	0.01	220 kJ/mol	0.032	150 kJ/mol	0.1	80 kJ/mol
θ	$2Q_{\text{ads}}$ [7]												
0.001	360 kJ/mol												
0.0032	290 kJ/mol												
0.01	220 kJ/mol												
0.032	150 kJ/mol												
0.1	80 kJ/mol												

effect of a change in this parameter on the overall results through a sensitivity analysis.

The adsorption activation energy tends to be much lower than the desorption activation energy and not to vary as much with coverage. For the analysis, the adsorption activation energy was assumed independent of coverage and the reference value was based on Ref. [14]. The activation energy of solution for the $\text{LiAlO}_2/\text{H}_2\text{O}$ system was also experimentally determined as being 23 kJ/mol from Ref. [14] and is used in this analysis.

Consideration of the relationships among the different surface activation energies allows a reasonable estimate of each surface activation energy to be made. Fig. 10 shows a potential energy diagram for atomic and molecular hydrogen at the ceramic breeder surface. From this diagram, the following relationships can be inferred among the different surface activation energies associated with each hydrogen atom or radical:

$$E_{\text{s}} = (E_{\text{diss}} - E_{\beta}) + (E_{\text{ads}} - E_{\text{des}}), \quad (33)$$

$$Q_{\text{ads}} = (E_{\text{des}} - E_{\text{ads}}). \quad (34)$$

The same relationships can also be derived by setting $R_{\beta} = R_{\text{diss}}$ and $R_{\text{ads}} = R_{\text{des}}$ at steady state from Eqs. (11), (13), (15) and (18), as described in detail in

Ref. [15]. In addition, the bulk to surface flux was assumed analogous to a diffusion step followed by an adsorption step and the reference value of E_β was set as the sum of the bulk diffusion activation energy and the adsorption activation energy.

Assuming that the surface fluxes can be reasonably characterized as shown above, the model can then be used to analyze the LiAlO_2 single crystal data in order to estimate the pre-exponential constant and the activation energy for the bulk diffusion coefficient. The robustness of the analysis can also be verified by determining through sensitivity analyses the effect on the results of varying key reference input parameters. The reference property data and input parameters assumed for the analysis are summarized in Table 2.

The heat of adsorption ($2Q_{\text{ads}}$ based on second-order process) for different coverages was estimated by fitting a curve to the data shown in Table 2, as illustrated in Fig. 11. For coverages, $\theta < 0.1$, the heat of adsorption decreases linearly with $\log \theta$. For coverages, $\theta > 0.1$, the heat of adsorption decreases with $\log \theta$ but would saturate at a value of about 40 kJ/mol [7]. For the analysis, for coverages, $\theta > 0.1$, the heat of adsorption was estimated from the following assumed curve fit to the heat of adsorption data, as illustrated in Fig. 11.

$$2Q_{\text{ads}} = 40(1 + (-\log \theta)^{3.5}). \quad (35)$$

6. Analysis of experimental data

Tritium release from LiAlO_2 single crystal was measured under two conditions [4,5]: isothermal annealing and constant heating rate experiments. MISTRAL-SC was used to analyze the isothermal annealing cases first in order to estimate the diffusion coefficient.

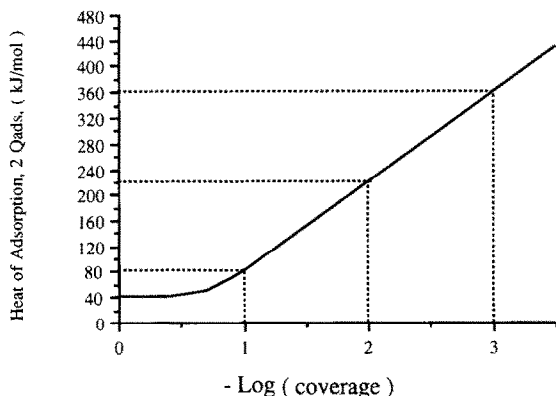


Fig. 11. Variation of heat of adsorption ($2Q_{\text{ads}}$) with coverage assumed in the analysis based on the data for the $\text{LiAlO}_2/\text{H}_2\text{O}(\text{g})$ system [7].

Sensitivity analyses were also performed to determine the effect of key parameters on the results. The model was then applied to the analysis of the constant heating rate experiments using the newly estimated bulk diffusion coefficient in order to confirm the validity of the estimate.

From the experimental data, the total tritium released from the single crystal was evaluated by the tritium release rate over the designated time using the trapezoidal rule. The total tritium released from the LiAlO_2 single crystal sample for the isothermal annealing and constant heating rate cases shown in Figs. 3 and 4 are 4.73×10^{15} atoms over 73 h, and 5.75×10^{15} atoms over 48 h, respectively. Assuming that all the tritium generated has been released during the out-of-pile anneals and that tritium was generated uniformly inside the crystal, the tritium generation rate was calculated as:

Tritium generation rate

$$= \frac{[\text{total tritium amount}]}{[\text{crystal volume}] \times [\text{irradiation time}]} \quad (36)$$

The model was then used to obtain the initial conditions based on the above tritium generation rate in the sample under irradiation. During irradiation, the single crystal sample was located inside a cylindrical capsule (38.1 mm long \times 6.35 mm diameter) [4]. The tritium generated in the sample would accumulate inside the sample and capsule during the irradiation time of ~ 10 h. The tritium inventory outside the sample in the capsule would probably be small since the diffusion of tritium in the LiAlO_2 single crystal is very slow at the low irradiation temperature ($< 200^\circ\text{C}$).

After irradiation, the capsule was removed from the reactor and kept at low temperature before the out-of-pile experiments begin. The tritium distribution inside the bulk, the coverage on the surface and the concentration inside the capsule at the end of irradiation can then be used as initial conditions when modeling the out-of-pile anneals, which started by having the capsule broken and by flowing the purge gas (Ar + 0.1% H_2). Note that all the tritium generated in the capsule was assumed to be released during the out-of-pile anneals. However, it might well be that a small amount of tritium would remain in the sample at the end of the anneals. To account for this possibility calculations were also done for the total tritium generated being slightly higher than the total out-of-pile tritium release.

Once the capsule is broken and the purge gas flows, the initial tritium concentration inside the capsule resides for a while around the sample before being swept by the purge gas. This tritium concentration would influence the adsorption to the surface of the sample for only a short time (of the order of 2–3 s based on

the capsule volume and the purge flow rate) but for completeness was included as an initial condition.

6.1. Tritium release during isothermal anneals

MISTRAL-SC was used to reproduce the experimental data shown in Fig. 2 based on the input parameters shown in Table 2. For each temperature anneal, the diffusion coefficient that best reproduces the results was determined. Three cases were run: case A, case B and case C. Case A refers to the initial tritium inventory set equal to the total out-of-pile tritium release, and cases B and C refer to the initial tritium inventory set 3% higher and 10% higher respectively than the total out-of-pile tritium release.

The modeling results indicate that about 7% of the tritium released at 538°C is released within 3 ms, mostly from the surface. This is not observed from the experimental results. However, this time constant is much smaller than the time response of the tritium measurement system, and, thus, even if this occurred during the experiment, its presence would not have been detected. In any case, its effect on the overall tritium release history and, thus, on the comparison of the modeling and experimental results is negligible.

Fig. 12 shows the results for case B. Values of the diffusion coefficient that best reproduce the tritium release profile at each temperature anneal are also shown. At 538°C, most of the tritium remains in the bulk and is released very slowly with almost a constant release rate. The tritium release from the surface, however, is fast and reaches a steady state level. When the temperature is raised to 777°C, the tritium release rate shows a high peak. This peak is about 50% higher

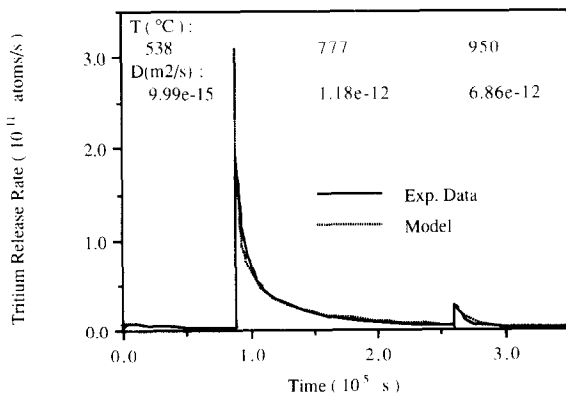


Fig. 12. Comparison of MISTRAL-SC results with the experimental results for tritium release from LiAlO_2 single crystal under three successive temperature anneals. The diffusion coefficient assumed for each temperature anneal is shown. The initial tritium inventory was set 3% higher than the total out-of-pile tritium release.

Table 3

Comparison of the total tritium release ($\times 10^{14}$ atoms) at each of the three temperature anneals with the modeling results assuming the initial tritium inventory is equal to 1.0 (case A), 1.03 (case B) and 1.1 (case C) the total tritium release during the out-of-pile anneals

	Annealing temperature		
	538°C	777°C	950°C
Experimental data			
Subtotal	3.665	39.48	4.269
Total	3.665	43.15	47.42
Case A			
Subtotal	3.664	39.49	1.518
Total	3.664	43.15	44.67
Case B			
Subtotal	3.606	40.61	3.962
Total	3.606	44.28	48.22
Case C			
Subtotal	3.672	39.50	7.262
Total	3.672	43.17	50.41

than the experimental data in this case. At this temperature, tritium in the bulk is transported to the surface faster than that at 538°C because of the higher diffusion coefficient. The surface inventory reaches a quasi steady-state level quickly and almost all of the tritium reaching the surface from the bulk is released to the purge.

At 950°C, the peak and profile of the output is almost the same as the experimental data. For case A, however, the tritium release was found to fall to a near-zero value quicker than the experimental data. This indicates that the assumption of some tritium left in the sample at the end of the out-of-pile anneals is probably reasonable. To further illustrate this, Table 3 shows a comparison of the total tritium release at each of the three temperature anneals with the modeling results for cases A, B and C. For each case, diffusion coefficients that best reproduce the tritium release profile at each temperature anneal have been used. The results indicate that the experimental tritium release during the 538 and 777°C anneals are quite well reproduced in all three cases. However, the tritium release during the 950°C anneal and, consequently, the total tritium release are best reproduced by case B. Case A underpredicts the experimental tritium release while case C overpredicts it, indicating again that the assumption that the initial tritium inventory is about 3% higher than the total out-of-pile tritium release is reasonable.

The diffusion coefficient, D , can be expressed as a function of the reciprocal of temperature, T , as follows:

$$-\ln D = -\ln D_0 + E_{\text{dif}}/RT. \quad (37)$$

Based on this, the three diffusion coefficients D_1 , D_2 and D_3 which best reproduced the tritium release results at each temperature anneal (see Fig. 12) were used to estimate the overall pre-exponential constant, D_0 , and activation energy of diffusion, E_{dif} . First, the negative of the logarithms of the three diffusion coefficients determined for each annealing temperature (538, 777 and 950°C) were plotted as a function of the reciprocal of temperature. The plot was then analyzed by the least square method to estimate E_{dif} from the gradient of the plot and the pre-exponential coefficient, D_0 , from the intersect with the y-axis ($-\ln D$). The resulting tritium diffusion coefficient, D_{sc} , for the LiAlO_2 single crystal is:

$$D_{sc} = D_0 \exp(-E_{dif}/RT) \\ = 1.29 \times 10^{-5} \exp(-141.5(\text{kJ/mol})/RT) (\text{m}^2/\text{s}). \quad (38)$$

Fig. 13 shows the comparison of output from the model with the experimental data using the diffusion coefficient of Eq. (38). The modeling results reproduce the experimental data very well except for the peak for the last anneal which is slightly higher than the experimental one.

Refs. [4] and [5] also show experimental results for the tritium release from similar LiAlO_2 single crystal under two successive anneals of 777 and 950°C. These results were also analyzed based on the input data of Table 2 and the diffusion coefficient of Eq. (38) in order to verify the adequacy of this D_{sc} . The results are shown in Fig. 14. Again, the tritium release experimental results are very well reproduced for both anneals.

The adequacy of this D_{sc} value was further tested through the analysis of the tritium release results from

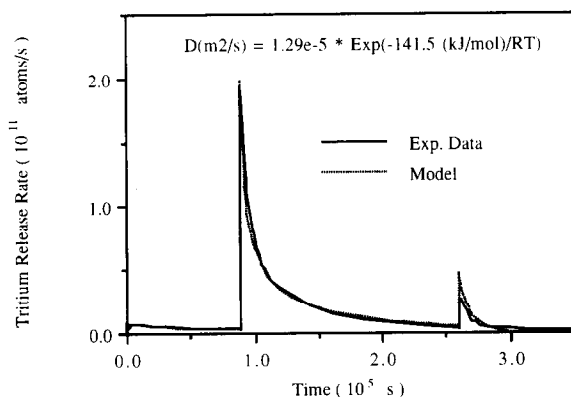


Fig. 13. Comparison of MISTRAL-SC results with the experimental results for tritium release from LiAlO_2 single crystal under three successive temperature anneals, based on D_{sc} of Eq. (38). The initial tritium inventory was set 3% higher than the total out-of-pile tritium release.

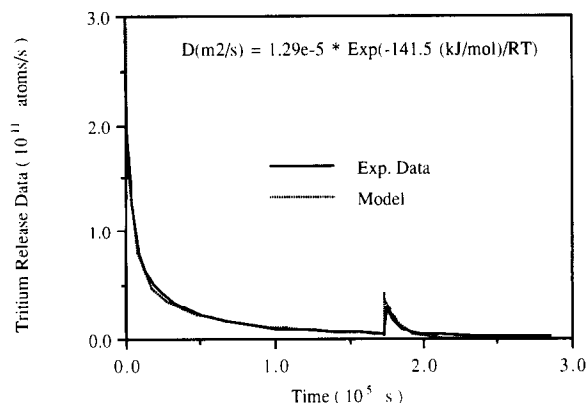


Fig. 14. Comparison of MISTRAL-SC results with the experimental results for tritium release from LiAlO_2 single crystal under two successive temperature anneals, based on D_{sc} of Eq. (38). The initial tritium inventory was set 3% higher than the total out-of-pile tritium release.

the constant heating rate experiments, as discussed in the next section.

6.2. Tritium release under constant heating rate conditions

The results for tritium release under a constant heating rate condition corresponding to 0.5 K/min (see Fig. 4) were analyzed using MISTRAL-SC based on the input data shown in Table 2 and on D_{sc} of Eq. (38). The initial inventory was assumed to be 3% higher than the total tritium release. The results are shown in Fig. 15. In general, the modeling results reproduce reasonably well the experimental results, including the shape of the tritium release profile, and

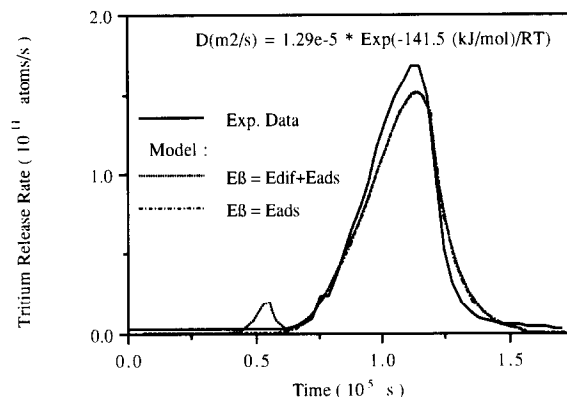


Fig. 15. Comparison of MISTRAL-SC results with the experimental results for tritium release from LiAlO_2 single crystal under a constant heating rate corresponding to 0.5 K/min, based on D_{sc} of Eq. (38). The initial tritium inventory was set 3% higher than the total out-of-pile tritium release.

the occurrence and slopes of the peak. However, the maximum tritium release obtained from the model is about 10% lower than the experimental value, which can still be considered reasonable based on input data and measurement uncertainties.

One interesting feature of the modeling results is the presence of a small tritium release peak after about 5×10^4 s, which is not observed experimentally. This peak seems to be caused by assumptions regarding the input data and will be discussed in the sensitivity analysis section.

6.3. Sensitivity analyses

Sensitivity analyses were performed to explore the effect on the modeling results of varying these input parameters from Table 2 with highest uncertainty and highest potential impact on the results, namely: (1) the activation energy for the flux from the bulk to the surface ($E_{\mathcal{F}}$); (2) the adsorption activation energy (E_{ads}); (3) the solution activation energy (E_s); and (4) the heat of adsorption (Q_{ads}).

6.3.1. Effect of $E_{\mathcal{F}}$ on the tritium release results

To derive the value for the activation energy for the bulk-to-surface flux ($E_{\mathcal{F}}$), the process was assumed to be analogous to a diffusion step followed by an adsorption step (see Fig. 10):

$$E_{\mathcal{F}} = E_{\text{dif}} + E_{\text{ads}} \quad (39)$$

However, if the tritium ion has already diffused to the surface site, the process could also be analogous to an adsorption step only, i.e.

$$E_{\mathcal{F}} = E_{\text{ads}} \quad (40)$$

In that case, a modified definition of E_{diss} from that shown in Table 2 needs to be used to preserve the activation energy balance, as illustrated in Fig. 10.

$$E_{\text{diss}} = E_s + E_{\mathcal{F}} + E_{\text{dif}} + Q_{\text{ads}} \quad (41)$$

The effect of these two definitions (Eqs. (40) and (41)) on the tritium release from the LiAlO_2 single crystal under constant heating rate conditions is also shown in Fig. 15. Except for $E_{\mathcal{F}}$ and E_{diss} , the same input parameters as shown in Table 2 were used. Interestingly, the modeling results are virtually unchanged except for the small tritium release peak previously seen at about 5×10^4 s which does not occur anymore.

The occurrence of this small peak seems to be anomalous and was further investigated. MISTRAL-SC was run with several different values of $E_{\mathcal{F}}$ between those of Table 2 and Eq. (40) for the same constant heating rate case shown in Fig. 15. The results indicate that as the value of $E_{\mathcal{F}}$ is decreased, the magnitude of the small tritium release peak decreases while its oc-

currence shifts to lower temperatures. It was found that this small peak tends to occur at a specific value of the ratio ($E_{\mathcal{F}}/T$). From the definition of the flux ($R_{\mathcal{F}}$) of tritium atoms entering the surface from the bulk, shown in Eq. (15), the ratio ($E_{\mathcal{F}}/T$) is included in the exponential term in the definition of $k_{\mathcal{F}}$. Under the given conditions, this exponential term seems to dominate the flux balance at the surface at this specific value of ($E_{\mathcal{F}}/T$).

The effect of the definition of $E_{\mathcal{F}}$ on the tritium release for the isothermal annealing case shown in Fig. 3 was also investigated. In this case, no visible effect was found as the modeling results were virtually identical to those shown in Fig. 13.

In general, this analysis indicates that the choice of $E_{\mathcal{F}}$ has a small effect on the modeling results for both the constant heating rate (except for the small tritium release peak discussed above) and isothermal annealing cases. Consequently, the value of D_{sc} estimated from the previous analysis would not be sensitive to the choice of $E_{\mathcal{F}}$ (within the reasonable range assumed above).

6.3.2. Effect of E_{ads} on the tritium release results

From Ref. [14], two different adsorption processes (probably physisorption and chemisorption) with different adsorption activation energies were distinguished over different temperature ranges. These results suggested a value of $2E_{\text{ads}}$ of about 6 kJ/mol in the range of 573–623 K, and about 30 kJ/mol in the range of 673–773 K. No data are available for E_{ads} at higher temperatures (> 773 K). Here, $2E_{\text{ads}} = 30$ kJ/mol was assumed since most of the release occurred within or above the 673–773 K range.

To determine the effect of the choice of E_{ads} on the results, MISTRAL-SC was run with the same input parameters as shown in Table 2 but for a range of $2E_{\text{ads}}$ values between 15 and 40 kJ/mol for the constant heating rate case shown in Fig. 4, and up to 70 kJ/mol for the temperature annealing case shown in Fig. 3. The modeling results were virtually unchanged from before. This is due in part to the relationship between the different surface flux activation energies (see Eqs. (33) and (34)). E_{ads} can be changed but the other activation energies would also change correspondingly based on their relationship for given values of E_s and Q_{ads} . This is an important feature of the surface flux model which helps to produce results which tend to be insensitive to changes in individual surface flux activation energy once E_s and Q_{ads} are defined. Since it is generally much easier to determine experimentally E_s and Q_{ads} than each individual surface flux activation energy, they tend to be the basis of the input data, resulting in reasonably robust model predictions.

6.3.3. Effect of E_s on the tritium release results

The solution activation energy, E_s , was estimated from the isotherms for hydroxide solubility in LiAlO_2 to be 23 kJ/mol OH^- in the temperature range of 400–600°C [14], which was used as the reference value in Table 2. However, no data are available for E_s at higher temperatures.

To ascertain the effect of E_s on the results, MISTRAL-SC was run for both the constant heating rate and constant temperature annealing cases for a range of E_s values between 15 and 40 kJ/mol. For the constant heating rate case, the results were unchanged. For the constant temperature anneal case, the only significant difference was a 50% higher local tritium release peak at the start of the 777°C anneal. The rest of the tritium release profile seemed unaffected.

As shown in Table 2, changing E_s affects the dissolution activation energy, E_{diss} . However, E_{diss} is already high enough that the tritium desorption flux is much higher than the tritium dissolution flux. Thus, changes in E_s would affect the dissolution flux but it is already relatively so small that the overall effect on the tritium release is small.

6.3.4. Effect of Q_{ads} on the tritium release results

In the 773–873 K range, for fractional surface coverages ranging from 0.001 to 0.1, the experimentally determined heat of adsorption ($2Q_{\text{ads}}$) for the $\text{LiAlO}_2/\text{H}_2\text{O}$ system ranges from approximately 360 to 80 kJ/mol [6], and was used as reference input here. For higher coverages, $2Q_{\text{ads}}$ was assumed to smoothly decrease to a minimum value of 40 kJ/mol, based on Eq. (34). Since most of the experimental tritium release would occur at higher coverages due to the presence of 0.1% H_2 in the purge, the effect on the results of assuming a constant value of $2Q_{\text{ads}} = 80$ kJ/mol was ascertained. Again, minimal effects ($\sim 1\%$ change) were observed on the modeling results.

Overall, the sensitivity analyses clearly indicate the robustness of the surface process model based on the relationship between the different activation energies, and, hence, of the results. Over a reasonable range of the various activation energies linked with the surface processes, the modeling results do not change significantly, which confirms the validity of the bulk diffusion coefficient estimated for the LiAlO_2 single crystal and shown in Eq. (38).

7. Sintered pellet diffusion coefficient

Refs. [4] and [5] describe the experimental tritium release results not only from LiAlO_2 single crystal specimens but also from LiAlO_2 sintered pellet specimens. MISTRAL-SC was adapted to a polycrystal situation by normalizing the surface fluxes to the BET surface area (based on Brunauer, Emmett and Teller

[16]) and used to analyze the tritium release data from the sintered pellet constant temperature anneal experiments. The LiAlO_2 sintered pellet had an average grain size of 84 μm , a BET surface area of 0.034 m^2/g , and a porosity of 30%. The results of the analysis indicated that the sintered pellet experimental results could not be reproduced with D_{sc} . This was confirmed by using the comprehensive model MISTRAL [1] for the same analysis. A reasonable reproduction of the results using the modified version of MISTRAL-SC could only be obtained with a diffusion coefficient lower than D_{sc} by a factor of about 200 (with the same activation energy of diffusion).

From the absolute rate theory, the diffusion pre-exponential constant can be expressed as [17]:

$$D_0 = a_0^2 \nu \exp(s^*/k), \quad (42)$$

where a_0 is the lattice constant, ν is the vibration frequency, s^* is the excess entropy, and k is Boltzmann's constant. Typically, ν is within one order of magnitude of 10^{13} s^{-1} and s^* is assumed to be zero, but could produce variation of up to one order of magnitude. This indicates that uncertainties exist in the value of D_0 . However, it is not clear why either of the variables determining D_0 in the single crystal case would be different in the polycrystal case.

A possible explanation for the difference between the single crystal and polycrystal diffusion coefficient could be that during irradiation, tritium might have only been generated in a thin layer only instead of uniformly across the single crystal. Thus, the diffusion coefficient estimated for the single crystal would tend to be higher as the characteristic diffusion length was based on the single crystal radius instead of on the thin tritium layer thickness. MISTRAL-SC was run again for the single crystal constant temperature anneal case for different thicknesses of such a layer and based on $D = D_{\text{sc}}/200$. The experimental results could be reasonably reproduced under the assumption of a thin tritium generation layer of thickness $\sim 30 \mu\text{m}$. However, even if the LiAlO_2 specimen contained 100% ^6Li , the mean free path of the thermal neutrons (0.025 eV) is about 0.4 mm, which precludes the assumption that tritium could only be generated in a 30 μm layer at the LiAlO_2 single crystal surface.

8. Comparison of diffusion coefficients

The diffusion coefficient of tritium in LiAlO_2 estimated for the single crystal is different not only from that estimated from the sintered pellet data but also from the "effective" diffusion coefficients estimated from previous experiments. These experiments used mostly sintered pellets under a variety of conditions which could cause other transport mechanisms to play a major role. Thus, the simple diffusion analysis of

Table 4

Summary of LiAlO₂ sample characteristics and of corresponding diffusion coefficients estimated from several tritium release experiments

Diffusion coefficient (D)	D_{sc}			
D_0 (m ² /s)	3.09×10^{-7}	1.29×10^{-5}	1.99×10^{-9}	8.9×10^{-7}
E_{diff} (kJ/mol)	80.9	141.5	90.4	197.9
D at 900 K (m ² /s)	6.23×10^{-12}	7.91×10^{-14}	1.13×10^{-14}	2.91×10^{-18}
Nature of sample	Solidified melt ^a	Single crystal	Crystalline powder ^b	Sintered pellet
Grain radius (μm)			6	10
Sample diameter (mm)	1.6–5.0 ^c	2	Particle size	4
Density (% of theoretical density)	97.3	100		77
Temperature range (K)	878–1178	811–1223	630–930	830–1173
Purge gas	Dry He	Ar + 0.1% H ₂		D ₂
Experiment type	Out-of-pile	Out-of-pile	Out-of-pile	In situ (VOM-22)
Characteristic length ^d	18.6 mm	1 mm	15.9 μm	1.65 mm
Reference	Bruning et al. [18]	Botter et al. [4]	Okuno, Kudo [19]	Kurasawa et al. [20]

^a Single particle;

^b 99% purity;

^c Average diameter = 3.3 mm;

^d Based on D_{sc} , $L = r_g \sqrt{D_{sc}/D}$.

these experiments would yield an “effective” diffusion coefficient that could include other effects. For completeness, assuming that diffusion were the controlling mechanism in these experiments, a simple analysis was performed to determine whether the “effective” diffusion path length in sintered pellet experiments could be different from the grain radius and more closely related to the sample dimension.

Table 4 shows a summary of LiAlO₂ sample characteristics and of corresponding diffusion coefficients estimated from several tritium release experiments. It can be seen that both the pre-exponential constant and the diffusion activation energy vary greatly over the different experiments. The table also shows the sample dimension for each case and, where available, the grain size for the sintered pellet cases. In addition, in each case, a characteristic length, L , is listed. L corresponds to the diffusion length based on D_{sc} from Eq. (38)

which would result in the same diffusive time constant as that obtained from the experimental diffusive path (equivalent to the grain radius, r_g) and the diffusion coefficient, D , estimated from the results

$$L = r_g (D_{sc}/D)^{0.5}. \quad (43)$$

There does not seem to be a consistent pattern linking the characteristic length so obtained to the sample dimension which could help to explain the large differences among the values of the diffusion coefficient. This would reinforce the belief that transport mechanisms other than diffusion played also a significant part in the tritium release in these experiments, thereby affecting the value of the “effective” diffusion coefficient estimated from the results.

Fig. 16 shows a graphical representation of the diffusion coefficient obtained from these different experiments as a function of temperature. The estimated values of the diffusion coefficient for the sintered pellet cases tend to be substantially lower than those from the single crystal cases, in concordance with the fact that a larger number of transport mechanisms are usually associated with sintered pellet cases than with single crystal cases.

9. Conclusions

Simple existing models were found not to adequately reproduce recent tritium release data for LiAlO₂ single crystal, indicating the need for a more comprehensive model. To help understand and interpret the data, a new model, MISTRAL-SC, was developed incorporating bulk diffusion as well as the four major surface processes and allowing for the variation

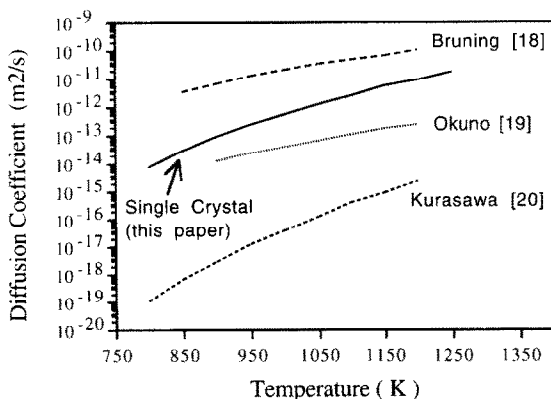


Fig. 16. Summary of diffusion coefficients for tritium in LiAlO₂.

of surface activation energies with coverage and for the presence of H_2 in the purge.

For given surface activation energies based on past experiments and analyses, a diffusion coefficient, D_{sc} , was estimated for the $LiAlO_2$ single crystal by reproducing the tritium release results for both isothermal anneals and constant heating rate conditions. Sensitivity analyses indicated minimal change in the calculated tritium release for both constant temperature anneals and constant heating rate conditions when E_β , E_{ads} , E_s , and Q_{ads} were varied over an appreciable and realistic range. This illustrates the robustness of the surface process model based on the relationship between the different surface activation energies.

Reproduction of the tritium release results for $LiAlO_2$ sintered pellets from the same set of recent experiments requires a bulk diffusion coefficient lower than that of the single crystal by a factor of about 200. A simple calculation indicates that self-shielding could not cause the single crystal diffusion coefficient estimate to be artificially low.

A comparison of diffusion coefficients estimated from several experiments was performed. Large variations exist in the estimates for the diffusion coefficient which tend to be appreciably higher when based on results from single crystal experiments than when based on results from sintered pellet experiments. To try to understand the discrepancies, a diffusive characteristic length was estimated in each case based on D_{sc} and on the effective diffusive time constant of the given experiment. However, no pattern linking this diffusive characteristic to the sample dimension clearly emerged. For past sintered pellet experiments, this could be explained since several tritium transport mechanisms could be at play. Performing a purely diffusive analysis on the tritium release data would then yield an "effective" diffusion coefficient which would include more than diffusion only and which would tend to be lower than the "true" bulk diffusion coefficient. However, for the recent set of sintered pellet data analyzed here, a comprehensive model including all the key bulk and surface tritium transport mechanisms was used and the resulting diffusion coefficient was still lower than D_{sc} by a factor of about 200.

Further effort is needed to try to understand the reason for this. Another $LiAlO_2$ single crystal experiment would be very useful to see if a similar tritium behavior in single crystal is observed. Single crystal experiments for other lithium ceramics would also help in the understanding. In the meantime, for $LiAlO_2$ experiment analysis it is suggested to use the diffusion coefficient for the single crystal, D_{sc} from Eq. (38). However, for $LiAlO_2$ blanket design analysis, to be conservative, use of a lower diffusion coefficient ($\sim D_{sc}/200$) is suggested.

10. Nomenclature

A	Area to volume ratio, = $3/a$	(m^{-1})
A_{ads}	Effective adsorption pre-exponential	(ms/kg)
A_{des}	Desorption pre-exponential	(s^{-1})
A_s	Surface area of the single crystal	(m^3)
a	Crystal radius	(m)
a_0	Lattice parameter of a FCC crystal	(m)
C_1, C_2	Constants in the desorption activation energy expression	(kJ/mol)
$C(r, t)$	Tritium concentration in the bulk	($atoms/m^3$)
C_p	Atom concentration in the purge gas	($atoms/m^3$)
C_0	Initial concentration in the crystal	($atoms/m^3$)
$D(T)$	Tritium diffusion coefficient in the bulk	(m^2/s)
D_0	Pre-exponential diffusion coefficient	(m^2/s)
E_{ads}	Activation energy of adsorption associated with each adsorbing atom or radical	(kJ/mol)
E_{des}	Activation energy of desorption associated with each desorbing atom or radical	(kJ/mol)
E_{dif}	Activation energy of diffusion per atom or radical	(kJ/mol)
E_{diss}	Activation energy for dissolution per atom or radical	(kJ/mol)
E_s	Activation energy of solution	(kJ/mol)
E_{\emptyset}	Activation energy for adsorption from bulk to surface per atom or radical	(kJ/mol)
F	Tritium release fraction	
G	Tritium generation rate	($atoms/m^3 s$)
h	Planck's constant	($J s$)
$J(t)$	Mass flux	($atoms/m^2 s$)
K_d	First-order desorption coefficient	(m/s)
K_{eq}	Equilibrium constant from Eq. (23) (≈ 4)	
K_r	Second-order desorption coefficient	(m^4/s)
k	Boltzmann's constant	(J/K)
k_{ads}	Rate constant for adsorption	(m/s)
k_{des}	Rate constant for desorption	($atoms/m^2 s$)
k_{diss}	Rate constant for dissolution	($atoms/m^2 s$)
k_{\emptyset}	Rate constant for bulk to surface flux	(m/s)
L	Characteristic diffusive length based on diffusive time constant and D_{sc} from Eq. (38)	(m)
M^i	Molecular weight of species i	(kg/mol)

N_{av}	Avogadro number	(molecules/mol)
N_s	Number of surface sites per unit area	(sites/m ²)
N_z	Number of adjacent sites (≈ 4)	
n_d	Order of adsorption/desorption	
P	Pressure in the purge	(Pa)
Q_{ads}	Heat of adsorption associated with each adsorbing atom or radical	(kJ/mol)
R	Universal gas constant	(kJ/mol K)
R_{ads}	Adsorption flux	(atoms/m ² s)
R_{des}	Desorption flux	(atoms/m ² s)
R_{dif}	Tritium bulk diffusion flux	(atoms/m ² s)
R_{diss}	Dissolution flux	(atoms/m ² s)
R_T	Tritium release rate	(atoms/s)
R_{∞}	Bulk to surface flux	(atoms/m ² s)
r	Radial coordinate	
r_g	Radius of grain	(m)
T	Absolute temperature	(K)
t	Time	(s)
V	Volume	(m ³)
V_p	Purge volume flow rate	(m ³ /s)
$V_{F,H}$	Volume fraction of protium in the purge	
x^i	mole fraction of species i	

Greek letters

α	Molecular ratio	
β	Linear heating rate	(K/s)
β_0	Pre-exponential factor	(m/s)
γ_j^i	Number of atoms of species j which adsorbs or desorbs per gas molecule of species i .	
σ	Condensation coefficient (≈ 0.4)	
θ^j	Surface coverage of j	

Subscripts and superscripts

i	Hydrogen molecule species
j, q	Hydrogen atom species
H	Protium
T	Tritium
m	Maximum
p	Purge
sc	Single crystal

Acknowledgement

This work was supported under US Department of Energy grant DE-FG03-86ER52123.

References

- [1] G. Federici, A.R. Raffray and M.A. Abdou, *J. Nucl. Mater.* 173 (1990) 184.
- [2] M.C. Billone, H. Attaya and J.P. Kopasz, *Modeling of Tritium Behavior in Li₂O*, ANL/FPP/TM-260, Argonne National Laboratory, Argonne, Illinois (August 1992).
- [3] F.M. Lord and J.S. Kittelberger, *Surf. Sci.* 43 (1974) 173.
- [4] F. Botter, J. Mougín, B. Rasneur, S. Tistchenko and J. Kopasz, *Mechanism of tritium release from lithium ceramics irradiated with neutrons*, 16th Symp. on Fusion Technology, September, 1990.
- [5] J.P. Kopasz, S. Tistchenko and F. Botter, *Ceramic Transactions: Fabrication and Properties of Lithium Ceramics III*, vol. 27 (1991) p. 315.
- [6] S. Cho and A.R. Raffray, *Modeling of Tritium Transport in LiAlO₂ Single Crystal*, ENG-93-20, UCLA-FNT-65, University of California, Los Angeles (1993).
- [7] A.K. Fischer and C.E. Johnson, *Fusion Technol.* 15 2B (1989) 1212.
- [8] B.M.W. Trapnell and D.O. Hayward, *Chemisorption*, 2nd ed. (Butterworths, London, 1964).
- [9] M. Boudart and G. Djega-Mariadassou, *Kinetics of Heterogeneous Catalytic Reactions* (Princeton University Press, 1984).
- [10] M.A. Pick and K. Sonnenberg, *J. Nucl. Mater.* 131 (1985) 208.
- [11] W.M. Jones, *J. Chem. Phys.* 17 (11) (Nov. 1949).
- [12] H.S. Carslaw and J.C. Jaeger, *Conduction of Heat in Solids* (Clarendon Press, Oxford, 1959) p. 234.
- [13] A.K. Fischer, *Fusion Technol.* 19 (3) Part 2A (May 1991) 1012.
- [14] A.K. Fischer and C.E. Johnson, *Adsorption, Dissolution and Desorption Characteristics of the LiAlO₂-H₂O (g) System*, DOE/ER-0313/3-7 (1987–1989).
- [15] A. Badawi, A.R. Raffray and M.A. Abdou, *Fusion Technol.* 21 (3) Part 2B (May 1992) 1939.
- [16] S. Brunauer, P.H. Emmett and E. Teller, *J. Am. Chem. Soc.* 60 (1938) 309.
- [17] D.R. Olander, *Fundamental Aspects of Nuclear Reactor Fuel Elements*, Technical Information Center, Office of Public Affairs, Energy Research and Development Administration, TID-267 11-P1 (1976).
- [18] D. Bruning, D. Guggi and H.R. Ihle, *The diffusivity of tritium in the system Li₂O-Al₂O₃*, Proc. 12th Int. Symp. on Fusion Technology, Julich, Germany, 1982.
- [19] K. Okuno and J. Kudo, *Fusion Eng. Des.* 8 (1989) 355.
- [20] T. Kurasawa et al., *J. Nucl. Mater.* 141–143 (1986) 265.